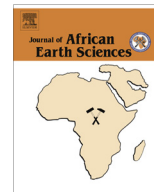




Contents lists available at ScienceDirect

Journal of African Earth Sciences

journal homepage: www.elsevier.com/locate/jafrearsci

Phase relationships and P – T path in NCFMASHTO system of the eclogite from the Tighsi area (Egere terrane, Central Hoggar, Algeria)

Sid Ali Doukkari^{a,*}, Khadidja Ouzegane^a, Amar Arab^a, Jean-Robert Kienast^b, Gaston Godard^b, Amar Drareni^a, Souad Zetoutou^a, Jean-Paul Liégeois^c

^a Lab. de Géodynamique, Géologie de l'Ingénieur et de Planétologie, FSTGAT-U.S.T.H.B., B.P. 32 El Alia, Dar el Beida, 16111 Alger, Algeria

^b JGP, 1 rue Jussieu, 75238 Paris Cedex 05, France

^c Geodynamics and Mineral Resources, Royal Museum for Central Africa, B-3080 Tervuren, Belgium

ARTICLE INFO

Article history:

Received 7 July 2013

Received in revised form 19 February 2014

Accepted 28 February 2014

Available online xxx

Keywords:

Hoggar

Egere

Eclogite

Thermodynamic modeling

Clockwise P – T path

ABSTRACT

The Tighsi area is situated in the northern part of the Egere-Aleksod terrane (Central Hoggar, South of Algeria). The eclogites and the garnet-amphibolites occur as lenses in marble, metapelite and quartzite. The petrological study shows that the high pressure paragenesis is characterized by the assemblage omphacite–garnet–rutile–quartz and epidote. Omphacite contains epidote, rutile and quartz inclusions. Due to the decompression, omphacite is the first mineral to destabilize into very thin symplectites of albite and clinopyroxene poorer of the jadeitic component. The paragenese of the lower pressure is represented by kelyphites and symplectites of amphibole–plagioclase separating garnet from omphacite and quartz. During this evolution, rutile transforms into ilmenite then, in the latest stage sphene replaces ilmenite. The thermodynamic modeling using THERMOCALC has confirmed these textural observations and suggests that the eclogites have experienced three stages of metamorphism. Stage I is the high pressure association, an H_2O under-saturated pseudosection adapted to this stage has been constructed in NCFMASHTO system. The association of high pressure corresponds to the field where garnet is in equilibrium with omphacite including epidote–rutile and quartz; The P – T conditions of 19.6 kbar and 694 °C have been estimated using the garnet core compositions. Stage II is the isothermal decompression where the amphibole–plagioclase kelyphites occur at the expense of garnet, omphacite and quartz at 15.5 kbar and 774 °C (conditions estimated using the garnet rim and the plagioclase–amphibole kelyphites compositions). Stage III is the late retrograde evolution; a second pseudosection with H_2O in excess has been constructed to model this stage and show the transformation of eclogites into garnet-bearing amphibolites and explains the occurrence of sphene. The P – T conditions of 9.3 kbar and 695 °C have been estimated using the compositions of the plagioclase with the maximum X_{an} and the amphibole with the minimum concentration of Al^{VI} . Both pseudosections show a clockwise path for eclogite evolution to garnet-amphibolites. This path characterizes the exhumation that succeeded a subduction event; therefore, the P – T path shows an isothermal decompression. Then, the geothermic gradients became normal so the decrease of pressure is accompanied with a decrease in temperature.

© 2014 Elsevier Ltd. All rights reserved.

1. Introduction

The Tuareg shield of the North Africa consists of the Adrar des Iforas massif (Mali), the Air massif (Niger) and the Hoggar massif (Algeria). This Pan-African belt has been formed during an early collision with the Saharan metacraton (SMC) between 750 and 650 Ma, and a later collision with the West African Craton (WAC) between 650 and 550 Ma (Bertrand and Caby, 1978; Black et al.,

1979; Caby et al., 1981; Liégeois et al., 1987). As a result, North–South mega shear zones have been formed during the post-collisional events. Referring to these major accidents, the Hoggar is divided into three main domains: The western, the central, and the eastern Hoggar. However, the paper of Black et al. (1994) has described the Tuareg shield as an amalgamation of 23 terranes lithologically and geochronologically different (Fig. 1a).

Very few studies on Hoggar eclogites have been published. In the LATEA (acronym of Laouni, Azrou N'Fad, Tefedest and Egere- Aleksod terranes) metacraton (Central Hoggar) garnet amphibolites and relict eclogites lenses can be followed from North to South and have been described in Aleksod (Sautter,

* Corresponding author. Tel.: +213 0779619808.

E-mail address: sidali.doukkari@gmail.com (S.A. Doukkari).

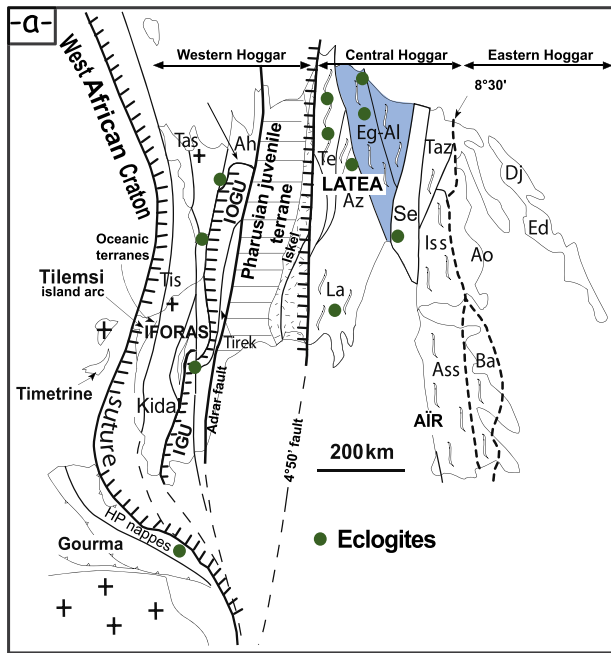


Fig. 1a. Schematic map of the Tuareg shield and the border areas after Cabyl (2003), showing eclogite location. Ah = Ahnet; Ao = Aouzegueur; Ass = Assodé; Ba = Barghot; Ed = Edembo; Dj = Djanet; Iss = Issalane; (Tas = Tassendjanet; Taz = Tazat; Se = Serouenout.

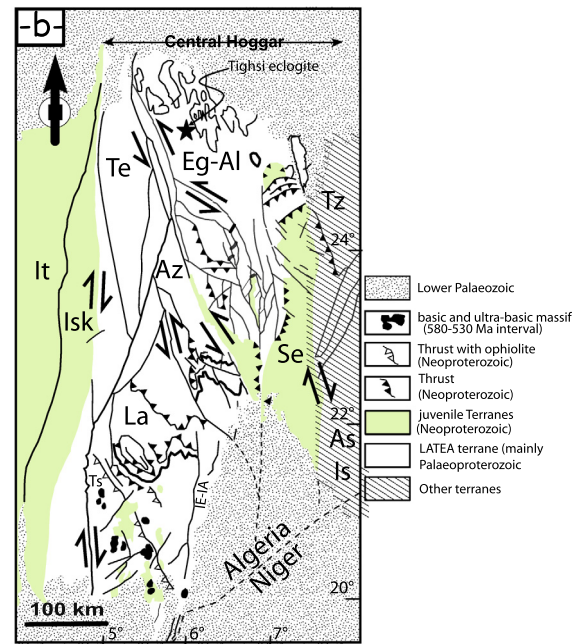


Fig. 1b. Sketch map of terranes from the Central Hoggar (Liégeois et al., 2003) showing the location of Tighsi area. Eg-Al = Egere-Aleksod; Te = Tefedest; Az = Azrou-n-Fad; Se = Serouenout; Is = Issalane; As = Assodé; La = Laouni; Isk = Iskel; It = In Teidini; Ts = Tessalit; Tz = Tazat; IE-IA = In Ebbegui-In Attei.

1985), Azrou N'Fad (Briedj, 1993; Zetoutou et al., 2004) and Laouni (Liégeois et al., 2003) terranes. Eclogite from Hoggar occurs also in the juvenile Pan-African area represented by the Tideridjaouine–Tileouine high-pressure metamorphic belt (Fettouh 2002; Berger, 2008) and Serouenout terrane (Derridj et al., 2010; Adjerid et al., 2012).

The eclogites from Tighsi (Egere-Aleksod terrane) preserve an exceptional sequence of reactions which best characterize the early high pressure metamorphic conditions and their later amphibolitisation. The purpose of this paper is to study the mineral assemblages and the relation between them; furthermore, thermodynamic modeling allows estimating P – T conditions and tracing the trajectory undergone during exhumation.

2. Geological setting

The Egere-Aleksod terrane is situated in Central Hoggar, more than 630 km North of Tamanrasset (South Algeria). The Central Hoggar is delimited by the 4° 50' and 8° 30' shear zones. In the western limit, the Iskel terrane overlaps the Central Hoggar (Fig. 1b), Iskel is considered, according to Liégeois et al. (2003), as a previous arc type terrane (850 Ma). The eastern limit, on the other hand, is characterized by the suture zone with the Saharan Metacraton. The studies of Liégeois et al. (2003) in Air (Niger) have led to interpret the central Hoggar as an old metacraton called LATEA (Laouni, Azrou-n-fad, Tefedest, and Egere-Aleksod); in addition to these four terranes, the terrane of Assode-Issalane has been added later to this metacraton.

Previous studies on this terrane (Lelubre, 1952; Duplan, 1972; Latouche, 1978) have revealed the presence of large domes and basins where orthogneissic anticlines are separated by spacious metasedimentary series synclines. The Paleoproterozoic basement areas are found in the Aleksod area, south of Egere region, where augen gneisses have been dated at c. 1940 Ma (Bertrand, 1974), this age is in good agreement with the Eburnean age of granite emplacement defined elsewhere in Africa (Bonhomme, 1962).

The age of the banded gneisses is not so well established: a Rb/Sr reference isochron (Bertrand and Lasserre, 1973) indicates an age of 2200 m.y., but isolated whole rock model ages suggest an older age (\approx 2500 m.y.). Thus there is some evidence of a pre-Eburnean history for this gneiss complex.

This terrane offers an exceptional region to study eclogites. Besides these mafic rocks, the Egere is characterized by an association of quartzite and magnetite-bearing quartzite, garnet-bearing metapelite, and dolomitic-siliceous marbles.

The Tighsi region (Fig. 2a) is located in the North-West part of the Egere-Aleksod terrane (Fig. 1b). The eclogites form meter- to hectometer-thick lenses or elongated-shaped bodies parallel to the foliation (Fig. 2c). These lenses are surrounded by meta-sedimentary rocks of marble, quartzite and metapelite (Fig. 2c and d). Furthermore, the large lenses conserve the eclogitic print; this is shown by the occurrence of green omphacite.

The contact between the eclogite lenses and their surrounding rocks is normal (Fig. 2d), this leads us to suppose that the protolith of these eclogites has been introduced during the deposit of the meta-sedimentary rocks.

3. Petrographic description

Three eclogite samples have been selected for this study (Gti2, Gti3, and Gti4). These rocks show complex textures as a result of the extremely heterogeneous mineral associations that developed in closely spaced domains during the various metamorphic stages. Textural relationships indicate the succession of three main metamorphic stages, which are described in detail below.

- (1) Stage I: the assemblage characterizing this stage consists of omphacite-garnet-quartz-rutile and epidote.
- (2) Stage II: the first mineral affected by the decompression is omphacite which is transformed into diopside + plagioclase.
- (3) Stage III: kelyphites of plagioclase and amphibole are formed around garnet; separating it from quartz and omphacite.

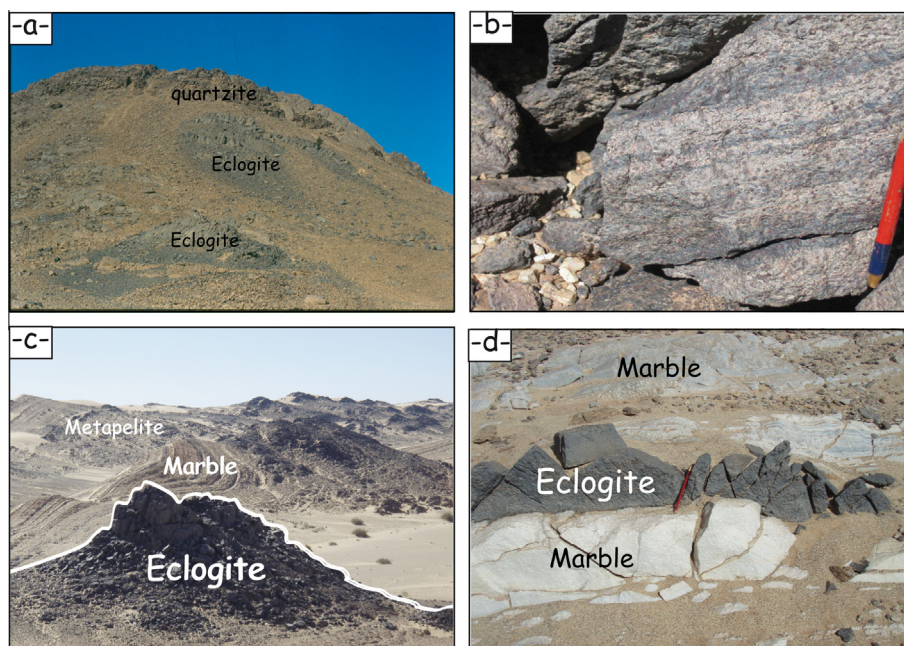


Fig. 2. Outcrop photographs from the Tighsi area (photographs by K. Ouzegane). (a): general view of the Tighsi hill with lenses of eclogites in quartzites (b): close up view of the eclogites which display the foliation defined by elongate rods of amphibole, (c): mega lenses of eclogites, where they form boudins stretched in the regional foliation of the folded metasedimentary rocks (d): eclogite lense surrounded by marbles.

- (4) Stage IV: this latest stage is characterized by very complex symplectites of diopside-amphibole-plagioclase.

During this complex evolution, rutile is transformed into ilmenite and then, in the latest stages of decompression, sphene replaces ilmenite (Fig. 2e).

3.1. Stage I

Thin sections have revealed that the minerals of this stage (garnet, omphacite and quartz), which represent the high pressure paragenesis (eclogite facies), are medium-grained and always separated by either amphibole-plagioclase kelyphites (i.e. stage III) or clinopyroxene-amphibole-plagioclase fine symplectites (i.e. stage IV, Fig. 3a). Garnet is very abundant, in large crystals that incorporate epidote, quartz and rutile inclusions in the core and become limpid toward rims (Fig. 3a). Omphacite, on the other hand, occurs as both preserved crystals, with quartz, epidote and rutile inclusions, or in relics of diopside-plagioclase symplectites, which is the most common (Fig. 3b). The inclusions in both garnet and omphacite may be ascribed to an earlier stage (prograde stage).

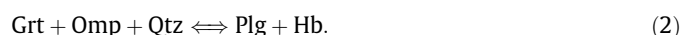
3.2. Stage II

Omphacite is transformed into very thin symplectites of diopside + plagioclase (Fig. 3b and d) which means that the eclogite (a metamorphic facies without plagioclase) is no more preserved. The transformation of omphacite suggests the reaction:

$$\text{Omp} + \text{Qtz} \rightleftharpoons \text{Plg} + \text{Di}. \quad (1)$$

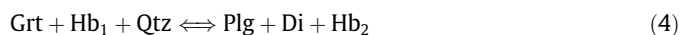
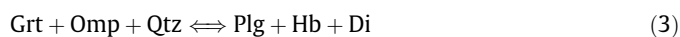
3.3. Stage III

During this stage coronas of plagioclase and amphibole are observed around garnet crystals. Their occurrence is the result of the reaction (2). These coronas are fine grained and amphibole is always green. These features suggest the following reaction:



3.4. Stage IV

Thin symplectites of either plagioclase diopside, or plagioclase diopside green amphibole are observed sometimes when omphacite is present (Fig. 3a and b) and other times without omphacite (Fig. 3c). These textures suggest the reactions:



4. Mineral chemistry

The chemical composition of the phases was determined using Cameca SX50 electron microprobe at the University of Paris VI with operating conditions of 15 kV, and 10 nA. Representative analyses of minerals are represented in Tables 1–4.

4.1. Garnet

The solid solution of garnets is dominated by almandine; where crystals are zoned with an increase of almandine from 55% to 61% (Table 1), balanced by a decrease of pyrope (17–10%), and grossular (31–25%) from core to rim, X_{Fe} ($X_{\text{Fe}} = \text{Fe}^{2+}/(\text{Fe}^{2+} + \text{Mg})$) ranges between 0.62 and 0.85. The plateau composition is probably related to equilibrium at peak metamorphism, whereas the rims re-equilibrated during retrogression, with a decrease in pyrope and grossular. The plotting of the compositions in the “pyrope, grossular, almandine + spessartine” diagram has revealed that they are C type eclogitic garnet, according to Coleman et al. (1965) classification (Fig. 4a).

4.2. Clinopyroxene

The compositions of the analyzed CpxI show that they are omphacite (Fig. 4b), where the jadeite content reaches 0.25 (Table 2). CpxII, on the other hand, shows compositions of diopside clinopyroxenes (Fig. 4b) with a lower jadeite content between

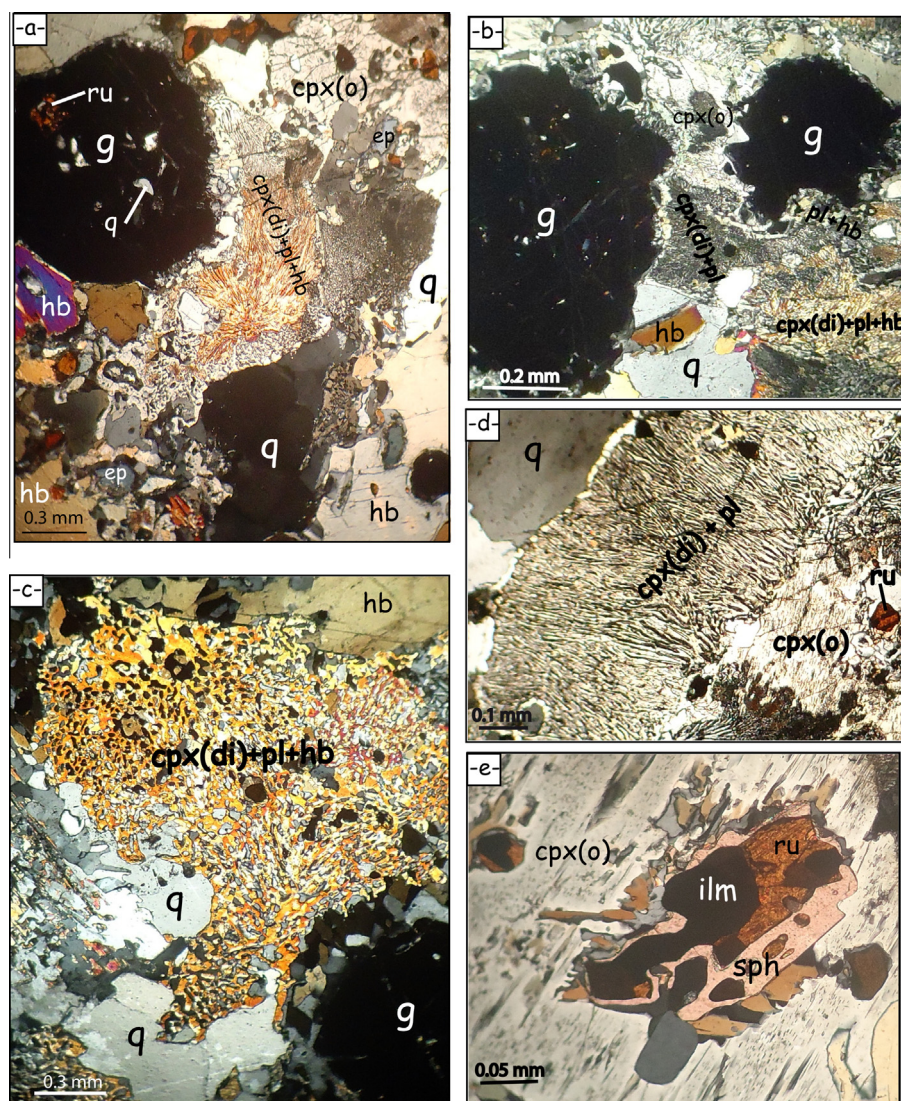


Fig. 3. Mineral assemblages and replacement textures. (a) Clinopyroxene hornblende-plagioclase symplectites replacing garnet-quartz-omphacite. (b) plagioclase and hornblende coronas around garnet, and omphacite destabilization into diopside-plagioclase symplectites. (c) Second generation of amphibole resulting from the reaction: $g + hb1 + q \rightleftharpoons hb2 + cpx(di) + pl$. (d) Thin symplectites of diopside and plagioclase. (e) Rutile destabilization into ilmenite then into sphene. Abbreviations: g: garnet; pl: plagioclase; q: quartz; hb: hornblende; cpx(o): omphacite; cpx(di): diopside; ep: epidote; ilm: ilmenite; ru: rutile; sph: sphene.

0.04 and 0.16 (Table 2). The transformation from CpxI to CpxII is manifested by a jadeitic substitution (Fig. 4c) where Ca, Fe and Mg replace Na and Al^{VI}.

4.3. Amphibole

X_{Fe} is between 0.32 and 0.39 (Table 3) and Fe^{3+}/Fe_T ranges between 0.07 and 0.56. Ti could reach 0.12 a.p.f.u. The Na content is generally lower than 0.79 a.p.f.u. The composition of these amphiboles indicates a titano-tschermakitic substitution ($Ti + 2Al^{IV} \rightleftharpoons Si + 2Mg$), with an increase of titanium and aluminum which occurs in a proportion of 1:1 (Fig. 4d).

4.4. Plagioclase

Plagioclase is always secondary with a composition that varies according to its textural position. It has a composition of oligoclase-andesine (An_{12}, Ab_{86}, Or_1 to An_{40}, Ab_{58}, Or_1) (Table 4) within the fine grained diopside-plagioclase symplectites and a labradorite, bytownite to anorthite (An_{60}, Ab_{40}, Or_0 to An_{93}, Ab_7, Or_0)

(Fig. 4e) within the plagioclase-amphibole kelyphites around garnet and epidote.

4.5. Epidote

The small grains of epidote in inclusion inside garnet and omphacite are very abundant. Epidote in the matrix, on the other hand, is clinozoisite. $Fe^{3+}/(Fe^{3+} + Al)$ is around 0.12.

The Fig. 4f represents the different eclogite's minerals in an Al/(Ca + Na) vs. Ca/(Ca + Na) diagram which helps in understanding the changes in mineralogy that occurred during the PT evolution. Clinopyroxene becomes richer in Ca during decompression and react with the garnet (I) to give hornblende, plagioclase and diopside (CpxII) symplectites (III). Moreover, the omphacite destabilization into plagioclase-diopside thin symplectites is confirmed (II).

5. Mineral equilibria modeling

Pseudosections have practically become a powerful approach to investigate mafic rocks. We show in this paper their power when

Table 1
Representative electron microprobe data of garnet.

Sample	Gti2 g(core)	Gti2 g(core)	Gti2 g(core)	Gti2 g(rim)	Gti2 g(rim)	Gti2 g(rim)	Gti3 g(core)	Gti3 g(rim)	Gti4 g(core)	Gti4 g(rim)
SiO ₂	39.77	37.00	37.65	37.72	38.40	37.00	38.58	37.75	37.28	37.76
TiO ₂	0.06	0.09	0.11	0.13	0.05	0.12	0.12	0.09	0.02	0.12
Al ₂ O ₃	22.45	21.00	21.07	21.72	21.65	21.00	21.44	21.52	21.16	21.25
Cr ₂ O ₃	0.05	0.00	0.00	0.02	0.05	0.06	0.01	0.00	0.02	0.11
FeO _t	22.51	26.00	26.81	26.69	25.97	28.00	23.86	25.90	25.40	26.71
MnO	0.03	0.44	0.09	0.76	0.08	0.73	0.15	0.82	0.25	1.68
MgO	7.73	4.00	3.24	3.04	4.05	3.00	4.49	2.75	2.53	3.09
NiO	0.00	0.00	0.00	0.00	0.00	0.00	0.00	0.00	0.12	0.00
CaO	8.40	10.00	10.39	9.20	9.89	9.00	10.85	10.31	12.24	9.31
Na ₂ O	0.00	0.00	0.01	0.05	0.07	0.02	0.00	0.04	0.00	0.07
K ₂ O	0.01	0.00	0.00	0.00	0.00	0.00	0.00	0.00	0.00	0.02
TOTAL	100.99	99.94	100.15	99.32	100.35	99.80	99.77	99.18	99.91	100.72
Num Ox	12.00	12.00	12.00	12.00	12.00	12.00	12.00	12.00	12.00	12.00
Si	3.01	2.94	2.98	2.99	3.00	2.96	3.02	3.00	2.96	2.98
Al ^{IV}	0.00	0.06	0.02	0.01	0.00	0.04	0.00	0.00	0.04	0.02
Al ^{VI}	2.00	1.91	1.95	2.02	1.99	1.94	1.98	2.01	1.94	1.95
Ti	0.00	0.01	0.01	0.01	0.00	0.01	0.01	0.01	0.00	0.01
Cr	0.00	0.00	0.00	0.00	0.00	0.00	0.00	0.00	0.00	0.01
Fe ³⁺	0.00	0.08	0.05	0.00	0.01	0.05	0.02	0.00	0.05	0.04
Fe ²⁺	1.42	1.64	1.73	1.77	1.69	1.82	1.54	1.72	1.63	1.73
Mg	0.87	0.47	0.38	0.36	0.47	0.36	0.52	0.33	0.30	0.36
Ni	0.00	0.00	0.00	0.00	0.00	0.00	0.00	0.00	0.01	0.00
Mn	0.00	0.03	0.01	0.05	0.01	0.05	0.01	0.05	0.02	0.11
Ca	0.68	0.85	0.88	0.78	0.83	0.77	0.91	0.88	1.04	0.79
Na	0.00	0.00	0.00	0.01	0.01	0.00	0.00	0.01	0.00	0.01
K	0.00	0.00	0.00	0.00	0.00	0.00	0.00	0.00	0.00	0.00
Total	8.00	8.00	8.00	8.00	8.00	8.00	8.00	8.00	8.00	8.00
X _{Mg}	0.38	0.22	0.18	0.17	0.22	0.16	0.25	0.16	0.15	0.17
Alm	0.48	0.55	0.58	0.60	0.56	0.61	0.52	0.58	0.55	0.58
Sps	0.00	0.01	0.00	0.02	0.00	0.02	0.00	0.02	0.01	0.04
Gr	0.23	0.28	0.29	0.26	0.28	0.26	0.30	0.29	0.35	0.26
Py	0.29	0.16	0.13	0.12	0.16	0.12	0.18	0.11	0.10	0.12

Table 2
Representative electron microprobe data of clinopyroxene.

Sample	Gti2 Cpx I	GTi2 Cpx II	GTi2 Cpx I	Gti2 Cpx II	Gti2 Cpx II	GTi3 Cpx II	GTi3 Cpx II	Gti4 Cpx I	Gti4 Cpx I
SiO ₂	54.44	53.72	53.53	52.10	52.40	50.98	49.38	51.23	51.54
Al ₂ O ₃	5.73	3.11	5.99	1.90	1.70	5.63	5.55	5.88	4.98
TiO ₂	0.19	0.17	0.14	0.10	0.10	0.19	0.26	0.11	0.20
Cr ₂ O ₃	0.00	0.13	0.11	0.10	0.20	0.00	0.09	0.00	0.00
FeO	8.77	7.20	6.44	10.10	7.60	7.83	8.37	10.36	10.72
MnO	0.10	0.10	0.11	0.00	0.10	0.00	0.00	0.09	0.11
MgO	9.44	13.23	11.43	12.00	12.60	11.31	11.31	9.57	10.08
NiO	0.00	0.00	0.00	0.00	0.00	0.17	0.06	0.00	0.06
CaO	16.69	21.97	19.89	21.90	20.90	21.28	22.21	17.43	18.30
Na ₂ O	3.99	1.00	2.59	1.00	1.20	1.30	1.12	3.13	2.47
K ₂ O	0.11	0.02	0.01	0.00	0.00	0.00	0.05	0.00	0.00
TOTAL	99.45	100.64	100.24	99.20	96.80	98.68	98.39	97.79	98.45
Num Ox	6.00	6.00	6.00	6.00	6.00	6.00	6.00	6.00	6.00
Si	2.01	1.97	1.95	1.96	2.00	1.91	1.86	1.93	1.94
Al ^{IV}	0.00	0.03	0.05	0.04	0.00	0.09	0.14	0.07	0.06
Al ^{VI}	0.25	0.11	0.21	0.05	0.08	0.16	0.11	0.19	0.16
Al ^t	0.25	0.13	0.26	0.08	0.08	0.25	0.25	0.26	0.22
Ti	0.01	0.00	0.00	0.00	0.00	0.01	0.01	0.00	0.01
Cr	0.00	0.00	0.00	0.00	0.01	0.00	0.00	0.00	0.00
Fe ³⁺	0.02	0.00	0.01	0.06	0.00	0.01	0.10	0.09	0.06
Fe ²⁺	0.25	0.22	0.19	0.26	0.24	0.24	0.17	0.23	0.28
Mg	0.52	0.72	0.62	0.67	0.72	0.63	0.64	0.54	0.57
Ni	0.00	0.00	0.00	0.00	0.00	0.01	0.00	0.00	0.00
Mn	0.00	0.00	0.00	0.00	0.00	0.00	0.00	0.00	0.00
Ca	0.66	0.86	0.78	0.88	0.86	0.86	0.90	0.70	0.74
Na	0.29	0.07	0.18	0.07	0.09	0.09	0.08	0.23	0.18
K	0.01	0.00	0.00	0.00	0.00	0.00	0.00	0.00	0.00
Total	4.00	4.00	4.00	4.00	4.00	4.00	4.00	4.00	4.00
X _{Mg}	0.67	0.77	0.77	0.72	0.75	0.78	0.79	0.70	0.67
Jd	24.80	7.24	18.40	4.58	7.68	9.47	8.41	19.69	16.44
Ac	4.63	0.65	1.01	5.90	1.52	0.98	5.76	10.02	5.21
Di + Ed + Pyr.Tsch.	70.56	92.11	80.59	89.51	90.79	89.55	85.84	70.29	78.35

Table 3
Representative electron microprobe data of amphibole.

Sample	Gti2 amp	Gti2 amp	Gti2 amp	Gti2 amp	Gti2 amp	Gti2 amp	Gti3 amp	Gti3 amp	Gti4 amp	Gti4 amp
SiO ₂	44.15	43.06	44.52	42.21	45.72	44.22	44.33	45.44	43.14	42.69
TiO ₂	0.70	0.35	0.86	0.69	0.68	0.79	1.01	0.41	0.71	0.61
Al ₂ O ₃	11.48	12.92	10.24	12.48	8.52	10.32	11.45	10.80	9.90	11.62
Cr ₂ O ₃	0.06	0.07	0.04	0.00	0.00	0.05	0.06	0.00	0.04	0.00
FeO	15.74	15.64	15.61	16.26	15.93	16.59	13.36	12.69	17.02	16.66
MnO	0.16	0.00	0.03	0.03	0.06	0.00	0.00	0.01	0.08	0.00
MgO	11.43	10.67	11.69	10.66	12.12	11.37	11.80	12.92	10.84	10.37
CaO	11.64	11.43	10.61	2.39	10.90	10.75	11.40	11.40	10.95	11.14
Na ₂ O	1.97	2.75	1.94	0.84	2.12	2.14	1.91	1.53	1.98	2.06
K ₂ O	0.49	0.01	0.88	0.01	0.59	0.78	0.55	0.55	0.68	0.65
Total	100.42	99.46	99.12	99.29	99.39	99.74	98.19	98.33	98.18	98.60
Num Ox	23.00	23.00	23.00	23.00	23.00	23.00	23.00	23.00	23.00	23.00
Si	6.48	6.39	6.59	6.31	6.78	6.54	6.59	6.68	6.52	6.44
AlIV	1.52	2.26	1.77	1.69	1.49	1.46	2.01	1.87	1.76	1.56
AlVI	0.46	0.65	0.38	0.51	0.26	0.34	0.60	0.55	0.29	0.50
Ti	0.08	0.04	0.10	0.08	0.08	0.09	0.11	0.05	0.08	0.07
Cr	0.01	0.01	0.00	0.00	0.00	0.01	0.01	0.00	0.01	0.00
Fe ³⁺	0.58	0.44	0.74	0.61	0.63	0.76	0.29	0.54	0.76	0.60
Mg	2.50	2.36	2.58	2.38	2.68	2.51	2.61	2.83	2.44	2.33
Fe ²⁺	1.35	1.50	1.20	1.42	1.35	1.29	1.37	1.02	1.39	1.50
Mn	0.02	0.00	0.00	0.00	0.01	0.00	0.00	0.00	0.01	0.00
Ca	1.83	1.82	1.68	1.78	1.73	1.70	1.82	1.80	1.77	1.80
Na	0.56	0.79	0.56	0.69	0.61	0.61	0.55	0.44	0.58	0.60
K	0.09	0.00	0.17	0.16	0.11	0.15	0.10	0.10	0.13	0.12
Total	15.48	16.26	15.77	15.63	15.72	15.51	16.06	15.88	15.76	15.53
X _{Mg}	0.65	0.61	0.68	0.63	0.67	0.66	0.66	0.74	0.64	0.61
Fe ³⁺ /Fet	0.56	0.23	0.38	0.30	0.32	0.37	0.18	0.35	0.35	0.29

Table 4
Representative electron microprobe data of plagioclase.

Sample	Gti2' Plg/CpxII	Gti2' Plg/CpxII	Gti2' Plg/amp	Gti2' Plg/CpxII	Gti2'' Plg/amp	Gti2' Plg/CpxII	Gti3 Plg/CpxII	Gti3 Plg/CpxII	Gti4 Plg/CpxII	Gti4 Plg/CpxII
SiO ₂	66.60	57.45	51.31	62.47	53.06	64.08	62.34	60.24	61.11	64.26
Al ₂ O ₃	22.43	26.98	30.98	21.79	30.43	21.73	24.28	24.90	24.73	22.24
TiO ₂	0.07	0.00	0.07	0.00	0.04	0.01	0.02	0.09	0.06	0.09
FeO	0.32	0.20	0.51	1.95	0.27	0.08	0.10	0.01	0.13	0.09
MnO	0.00	0.00	0.00	0.00	0.00	0.00	0.06	0.01	0.00	0.00
MgO	0.01	0.00	0.14	0.24	0.00	0.00	0.05	0.00	0.00	0.03
CaO	2.63	8.89	12.71	3.84	12.03	2.87	4.96	6.62	5.45	3.34
Na ₂ O	10.27	6.86	4.62	8.87	4.62	10.24	8.92	7.99	8.92	10.12
K ₂ O	0.22	0.08	0.02	0.47	0.03	0.44	0.13	0.14	0.11	0.05
TOTAL	102.56	100.51	100.37	99.64	100.47	99.46	100.88	100.14	100.57	100.23
Num Ox	32.00	32.00	32.00	32.00	32.00	32.00	32.00	32.00	32.00	32.00
Si	11.45	10.27	9.31	11.20	9.56	11.40	10.97	10.73	10.82	11.33
Al	4.55	5.68	6.63	4.61	6.46	4.56	5.03	5.23	5.16	4.62
Ti	0.01	0.00	0.01	0.00	0.01	0.00	0.00	0.01	0.01	0.01
Fe ³⁺	0.05	0.03	0.08	0.29	0.04	0.01	0.01	0.00	0.02	0.01
Mn	0.00	0.00	0.00	0.00	0.00	0.00	0.01	0.00	0.00	0.00
Mg	0.00	0.00	0.04	0.06	0.00	0.00	0.01	0.00	0.00	0.01
Ca	0.48	1.70	2.47	0.74	2.32	0.55	0.94	1.26	1.03	0.63
Na	3.42	2.38	1.63	3.08	1.61	3.53	3.04	2.76	3.06	3.46
K	0.05	0.02	0.01	0.11	0.01	0.10	0.03	0.03	0.03	0.01
Total	20.01	20.08	20.18	20.09	20.01	20.14	20.04	20.02	20.13	20.08
X _{An}	0.12	0.417	0.60	0.19	0.59	0.13	0.24	0.31	0.25	0.15
X _{Alb}	0.87	0.580	0.40	0.78	0.41	0.85	0.76	0.68	0.74	0.84
X _{Orth}	0.01	0.005	0.00	0.03	0.00	0.02	0.01	0.01	0.01	0.00

we attempt to trace the *P–T* path pursued by the Tighsi area eclogites.

THERMOCALC version 3.33 (Powell and Holland, 1988; updated June 2009), using the 2003 updated version of the Holland and Powell (1998) data set (file tc-ds55.txt), has allowed the calculation of the *P–T* pseudosections in the Na₂O–CaO–FeO–MgO–Al₂O₃–SiO₂–H₂O–TiO₂–Fe₂O₃(NCFMASHTO) chemical system. Thermodynamic models of the phases used in the calculations are: hornblende, actinolite and glaucophane (Diener et al., 2007;

updated by Diener and Powell, 2012), omphacite and diopside (Green et al., 2007; updated by Diener and Powell, 2012), garnet (White et al., 2007), epidote (Holland and Powell, 1998), plagioclase (Holland and Powell, 2003), ilmenite (White et al., 2000). Rutile, sphene, quartz and H₂O are pure end-member phases.

The MnO, Cr₂O₃, P₂O₅ and K₂O (K₂O of the studied samples is less than 0.2%) were excluded to enable the calculation of the pseudosections in the NCFMASHTO system. The Fe₂O₃ is obtained by the converting of 15% to 20% of the Fe total into Fe³⁺ because the

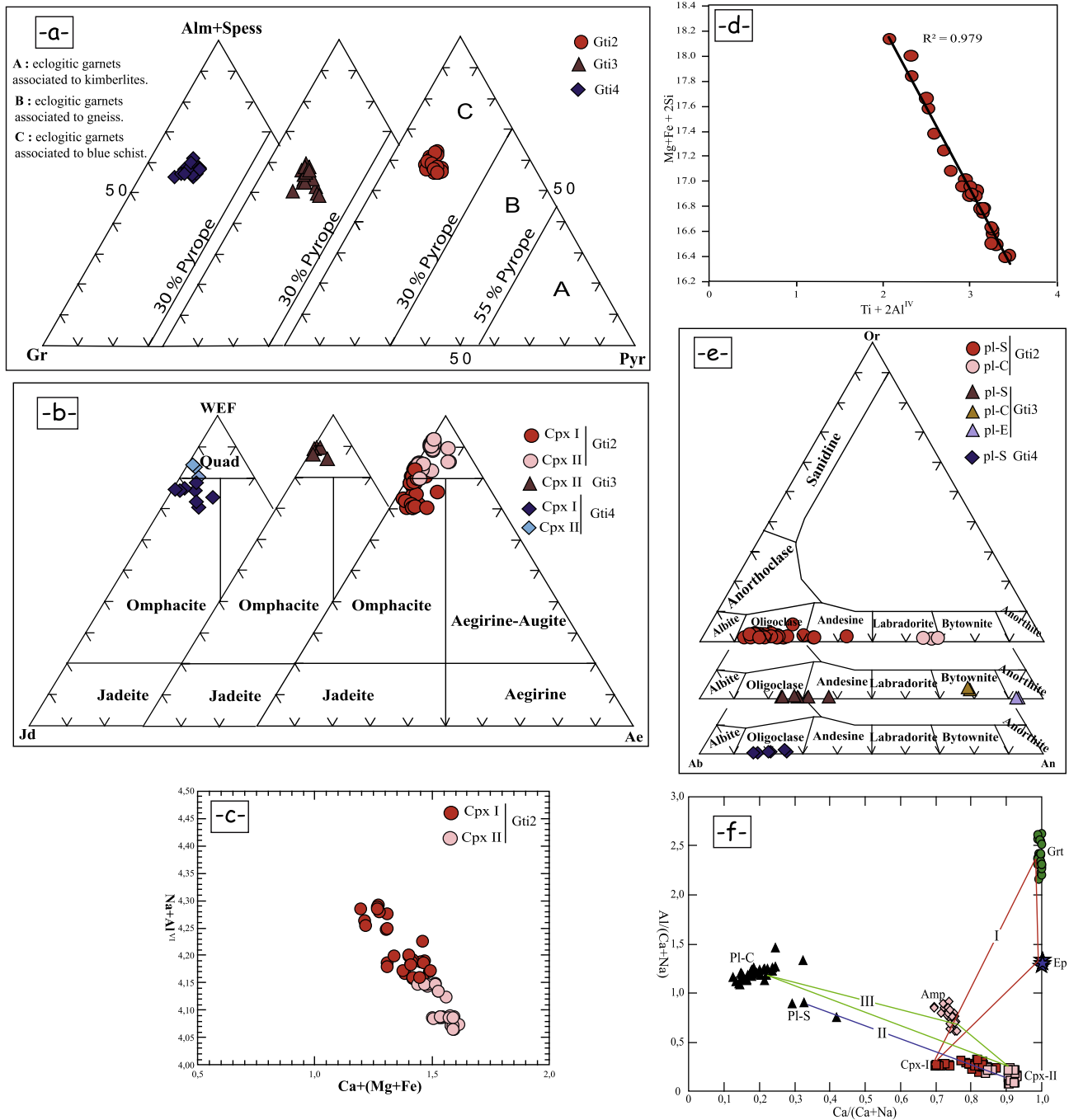


Fig. 4. (a) Garnet compositions plotted in the (almandine + spessartine)-grossular-pyrite diagram of Coleman et al. (1965). (b) Clinopyroxene compositions plotted in the (wollastonite + enstatite + ferrosilite)-jadeite-aegirine diagram of Morimoto (1988). (c) jadeitic substitution in clinopyroxene (Na + Al vs. Ca + Mg + Fe). (d) titanoschermakitic substitution (Ti + 2Al^{IV} vs. Si + 2Mg) in amphiboles. (e) Plagioclase compositions plotted in the albite-anorthite-orthoclase diagram. (f) Al/(Ca + Na) vs. Ca/(Ca + Na) diagram showing the chemical compositions of the mineral phases and the different observed mineral assemblages. Abbreviations: pl-S: plagioclase in symplectites with amphibole around garnet; pl-C: plagioclase from epidote destabilization; Cpx I: primary clinopyroxene (omphacite); Cpx II: secondary clinopyroxene (diopside).

ilmenite is the main oxide and the magnetite is rarely present (Diener and Powell, 2010).

In order to determine the peak metamorphic conditions and trace the path undergone by the eclogites of the Tighsi area, a pseudosection has been constructed using a bulk composition obtained from the whole-rock composition of the Gti2 sample (SiO₂ = 48.39 wt%, TiO₂ = 1.44 wt%, Al₂O₃ = 15.56 wt%, Fe₂O₃ = 13.7 wt%, MgO = 6.52 wt%, MnO = 0.19 wt%, CaO = 11.87 wt%, Na₂O = 1.99 wt%, K₂O = 0.24 wt%, P₂O₅ = 0.21 wt%, Total = 99.85).

Whole-rock major elements data were obtained by using ICP-AES (CRPG-CNRS), at Nancy; France. This pseudosection is calculated at 500–950 °C and 14–22 kbar (Fig. 5a), it is composed by trivariant to sixth variant fields. Boundary lines are pressure-dependent. The occurrence of garnet and quartz in all fields is worthy of note with the mineral assemblage of garnet, omphacite, rutile, epidote and quartz at high pressure as the peak metamorphic paragenesis. At low temperature (<800 °C), hornblende is the first mineral that occurs when the pressure decreases; plagioclase, on the other

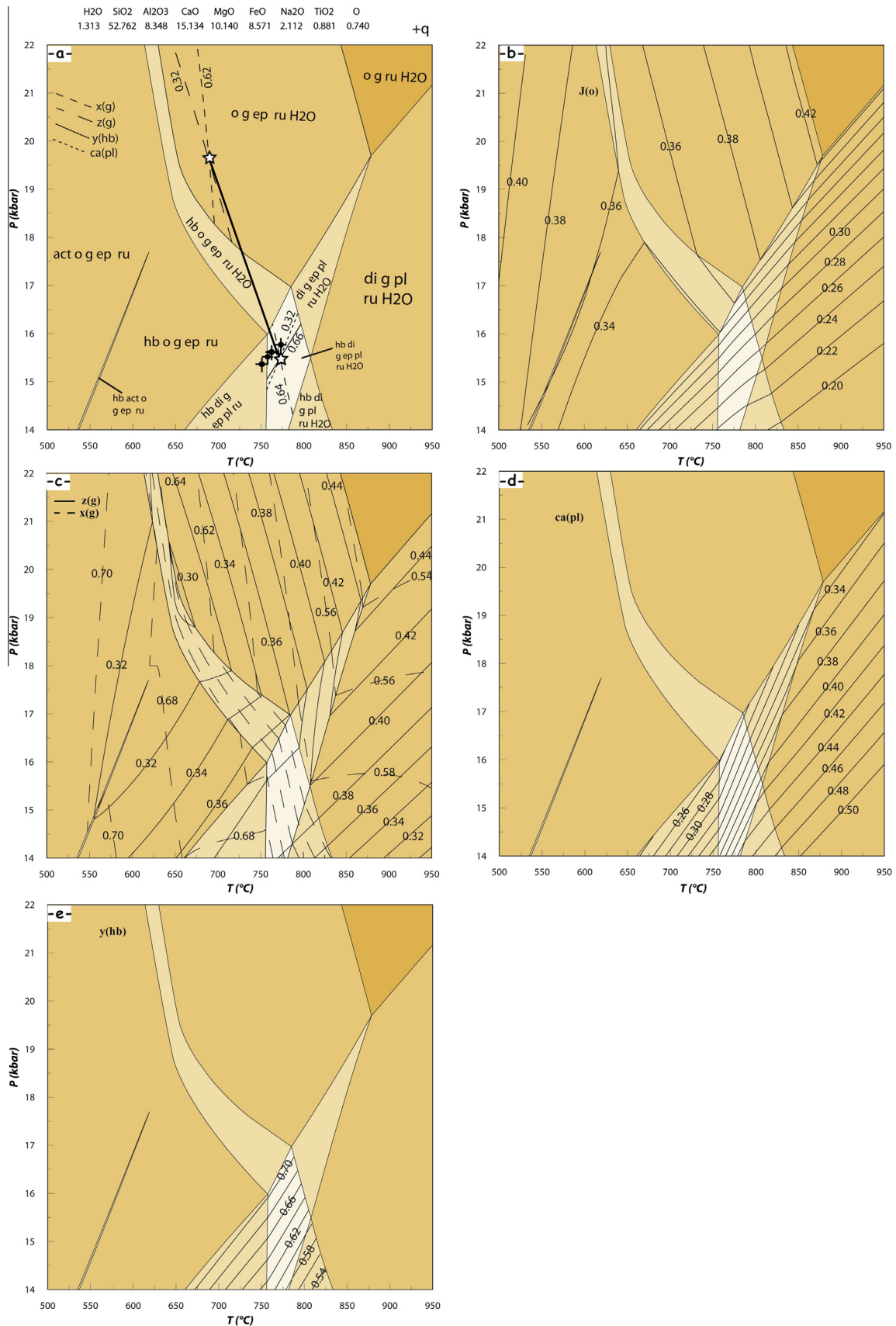


Fig. 5. P – T pseudosections for the sample Gti2. (a) the H_2O under-saturated conditions ($M_{H_2O} = 1.31$ mol%). White stars represent the metamorphic conditions obtained by the intersection of $X(g)$, $z(g)$, $ca(pl)$ and $y(hb)$ calculated from electron microprobe analyses on thin sections, $ca(pl) = Ca/(Na + Ca)$, $x(g) = Fe/(Fe + Mg)$, $z(g) = Ca/(Ca + Fe + Mg)$, $y(hb) = Al^{VI}$. The retrograde path is represented by a thick line. The black circles represent the P – T conditions obtained using the average P – T method. (b) The evolution of the $J(o)$ in the P – T space. (c) The evolution of the $x(g)$ and $z(g)$ in the P – T space. (d) The evolution of the $ca(pl)$ in the P – T space. (e) The evolution of the $y(hb)$ in the P – T space.

hand, appears the first at high temperature. Moreover, this H₂O under-saturated pseudosection is characterized by epidote-bearing fields at low temperature/high pressure side; however, epidote disappears at high temperature/low pressure.

Isopleths representing the composition of clinopyroxene ($J(\text{cpx}) = \text{Na}/(\text{Na} + \text{Ca})$), garnet ($X(\text{g}) = \text{Fe}/(\text{Fe} + \text{Mg})$), and $z(\text{g}) = \text{Ca}/(\text{Ca} + \text{Fe} + \text{Mg})$), plagioclase ($\text{ca}(\text{pl}) = \text{Ca}/(\text{Ca} + \text{Na})$) and hornblende ($y(\text{hb}) = \text{Al}^{\text{VI}}$) are shown in Fig. 5. $J(\text{cpx})$ increases proportionally with the rise of pressure. In the plagioclase-bearing fields, at low pressure, $J(\text{cpx})$ is pressure-dependent; however, at high pressure, it becomes more temperature-dependent with a remarkable decrease at low temperature side (fields without H₂O, Fig. 5b). $X(\text{g})$ increases from the low temperature/low pressure side to the high temperature/high pressure side (Fig. 5c). $Z(\text{g})$ gets its highest values at the epidote line and decreases away from that line on the both sides (Fig. 5c). Plagioclase is stable at high temperature low pressure side; therefore, the $\text{ca}(\text{pl})$ increase toward high temperature/low pressure. Amphibole, in the other hand, is stable at low temperature/high pressure, $y(\text{hb})$ decrease toward high temperature.

Significantly, the analyzed clinopyroxene, where the maximum of $J(\text{cpx})$ is 0.24 (Table 2), failed to register the early conditions because of its relatively smaller grain size, the chemistry of clinopyroxene underwent re-equilibration during decompression. $X(\text{g})$ and $z(\text{g})$ isopleths in garnet have different orientation in P T space. $X(\text{g})$ garnet decreases from the core to the rims between (0.84 and 0.62) and $z(\text{g})$ garnet is between 0.25 and 0.32. The compositional parameters $X(\text{g})$ and $z(\text{g})$ contents are proved to be robust to constrain the metamorphic conditions of eclogites. This is because the re-equilibrated garnet owing to its much larger volume relative to the symplectites. Also diffusion of Ca in garnet is extremely sluggish (Chakraborty and Ganguly, 1991). The intersection of $z(\text{g})$ isopleth of 0.32 (the maximum $z(\text{g})$ calculated from the analyzed garnets) with $X(\text{g})$ of 0.62 (the minimum of $X(\text{g})$ calculated from the analyzed garnets) succeeds to record the peak metamorphic conditions of eclogites which are 19.6 kbar and 694 °C (Fig. 5a). This garnet composition predicts that omphacite coexisting with quartz, garnet, epidote and rutile would have a composition of $J_{\text{d}} 36$, 12 mol% higher than that maximum measured ($J_{\text{d}} 24$). The first appearance of amphibole–plagioclase coronas around garnet has indicates 15.5 kbar, 774 °C as P – T conditions (this conditions correspond to the highest $y(\text{hb})$ in the analyzed amphiboles).

A second pseudosection has been calculated with H₂O saturated (Fig. 6). This pseudosection is applicable to the retrograde path if H₂O infiltrates through veins to keep the eclogite completely hydrated. Fig. 6 shows the H₂O-saturated pseudosection constructed for the P – T range 8–13 kbar and 600–750 °C. The assemblages on the high temperature side of the pseudosection may be metastable with respect to assemblages involving melt (melting model is not yet available for mafic rocks); therefore, the pseudosection was truncated at 750 °C. The variance of fields changes from tri to hexa. Garnet is stable on the high temperature high pressure side. Plagioclase disappears at low temperature high pressure; however, epidote is stable only on the high pressure low temperature side. At low pressure, rutile transforms into sphene.

In order to follow the evolution of the minerals' composition, isopleths, representing the composition of clinopyroxene ($J(\text{di})$), plagioclase ($\text{Ca}(\text{pl})$), garnet ($X(\text{g})$ and $z(\text{g})$) and amphibole ($a(\text{hb})$, $y(\text{hb})$ and $z(\text{hb})$), where $a(\text{hb}) = X_{\text{Na}}$, A and $z(\text{hb}) = X_{\text{Na}}$, M4. see caption of Fig. 6 for notation and abbreviations.), have been constructed and are represented in the Fig. 6a–d.

The Fig. 6b is contoured for both $J(\text{cpx})$ in clinopyroxene and $\text{ca}(\text{pl})$ in plagioclase. The composition of clinopyroxene as symplectites with plagioclase in the retrogressed eclogites has $J(\text{cpx})$: 7–20 (Table 2). Plagioclase is not stable at high pressure low temperature part; however, it becomes stable upon decompression

with a composition of An12–An60 which is consistent with the observed mineral compositions. The Fig. 6c, on the other hand, represents the isopleths of garnet ($z(\text{g})$ and $X(\text{g})$) which have always a different orientation in PT space. $X(\text{g})$ values are relatively high: 0.74–0.88 contrary to $z(\text{g})$: 0.32–0.44. These garnet compositions ($X(\text{g})$) correspond to the rims of the analyzed garnets (Table 1). The evolution of the amphibole composition ($a(\text{hb})$, $y(\text{hb})$ and $z(\text{hb})$) is shown in Fig. 6d. The composition of amphibole as large grains or as kelyphites with plagioclase surrounding garnet in the garnet-bearing amphibolites has a $y(\text{hb})$: 0.26–0.65 (Table 3), this is consistent with the isopleths values.

The P – T evolution is constrained by comparing observed textures and measured mineral compositions with calculated isopleths of compositional parameters. Therefore, the peak metamorphic conditions of 19.6 kbar, 694 °C (Fig. 5a) have been obtained using the core compositions of analyzed garnets. The highest value of $J(\text{o})$ that has been analyzed (0.24) is in equilibrium with $X(\text{g}) = 0.64$, $\text{ca}(\text{pl}) = 0.32$ and $y(\text{hb}) = 0.66$ this gives 15.5 kbar and 770 °C. At the latest stages, omphacite is destabilized into diopsidic clinopyroxene–plagioclase symplectites; the maximum of $\text{ca}(\text{pl})$ component (0.42) with $j(\text{di}) = 0.18$ isopleth (Fig. 6a) reveal the conditions of 12.5 kbar, 730 °C. $X(\text{g}) = 0.84$ (corresponds to the rims of the analyzed garnets) is in equilibrium with $y(\text{hb}) = 0.46$ amphibole and $\text{an}(\text{pl}) = 0.60$ analyzed plagioclase at 9.3 kbar and 695 °C conditions.

6. Discussion

The phase relations are very sensitive to the bulk composition. For example, if omphacite is taking up slightly too much Si, it will deplete the remaining bulk composition in Si and the eclogite might be calculated to be quartz-absent even when the natural example contains minor quartz. The amphibole model does not currently include K or Ti substitution, a melt model for mafic rocks is not yet available, and the clinopyroxene model does not include tetrahedral site Al (Diener and Powell, 2012). Despite of all these uncertainties, the thermodynamic modeling stills a very powerful approach to study mafic rocks. Therefore, the data presented above indicate that the eclogites of Tighsi underwent a two-stage exhumation evolution.

6.1. Isothermal decompression

This stage is represented by solid black arrow in Fig. 5a. It characterizes the passage from the peak conditions of 19.6 kbar–694 °C to 15.5 kbar–770 °C. These estimates are the first for this terrane and for the LATEA eclogites using modern mineral equilibria methods. The first plagioclase appears following to the omphacite destabilization with giving up on its Na becoming more and more over rich in Ca. Garnet, on the other hand, presents a zoning with a decrease in pyrope and grossular balanced by an increase in almandine component. These chemical observation are confirmed by the pseudosections where $z(\text{g})$ and $J(\text{o}/\text{di})$ decrease but $X(\text{g})$ increase towards low pressure (Fig. 5).

6.2. Cooling decompression

This stage represents the transformation of eclogites to actual garnet amphibolites. It is characterized by hydrous mineral parageneses (amphibole and sphene); therefore, the pseudosection calculated to model this final decompression is H₂O saturated. The symplectites are featured Ca rich plagioclase and clinopyroxene.

This P – T path characterizes the exhumation that succeeded a subduction event; therefore, it shows an isothermal decompression that could be explained by the rapid coming back toward

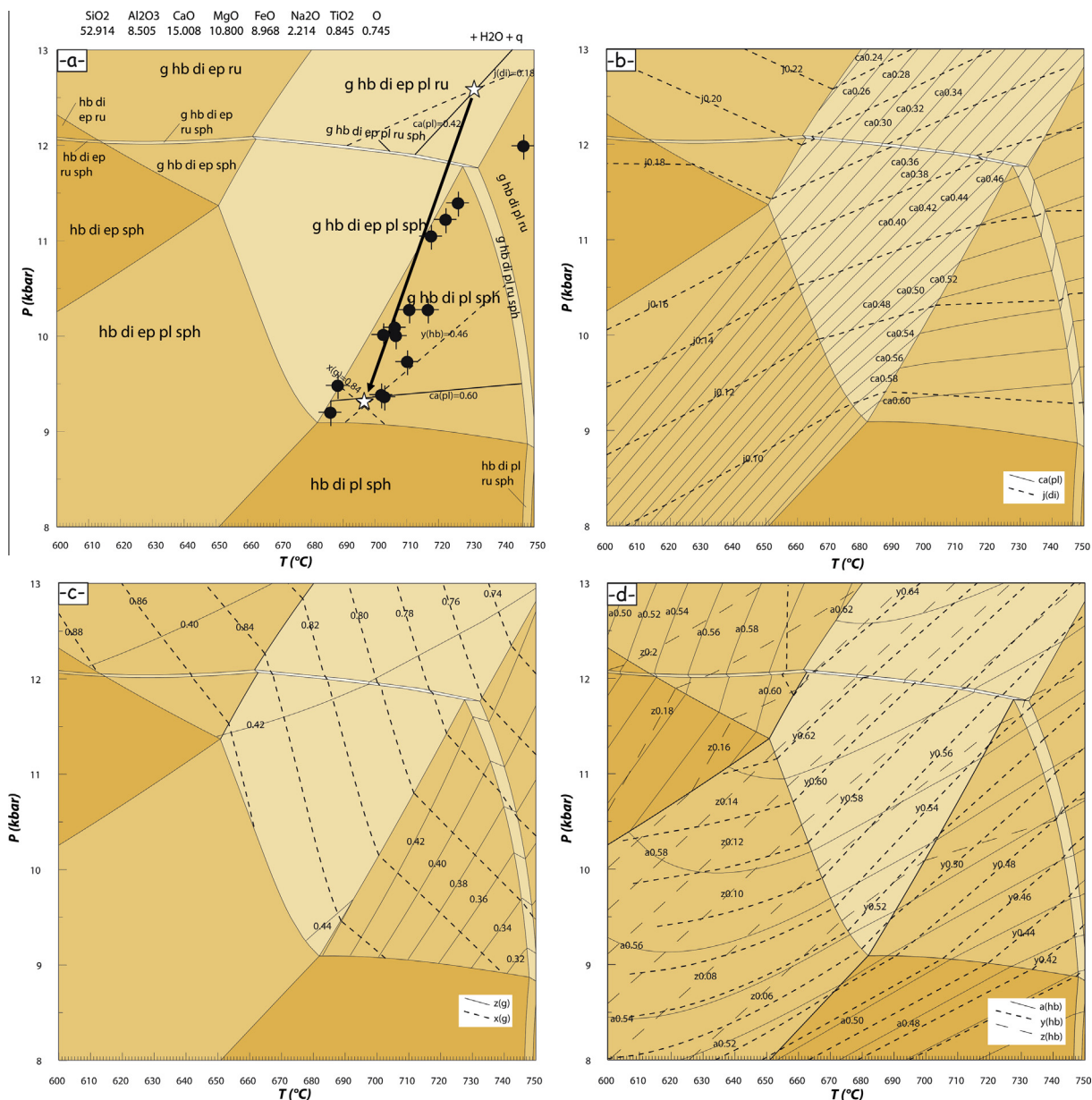


Fig. 6. P – T pseudosections for the sample Gti2. (a) The H_2O saturated conditions (H_2O in excess), white stars represent the metamorphic conditions obtained by the intersection of $j(di)$, $Ca(pl)$, $X(g)$ and $y(hb)$ calculated from electron microprobe analyses on thin sections, $j(di) = Na/(Na + Ca)$; $X(g) = Fe/(Fe + Mg)$ and $Ca(pl) = Ca/(Ca + Na)$ and $y(hb) = Al^{VI}$. The retrograde path is represented by a thick line. The black circles represent the P – T conditions obtained using the average P – T method. (b) The evolution of the $j(o)$ and $ca(pl)$ in the P – T space. (c) The evolution of the $X(g)$ and $z(g)$ in the P – T space. (d) The evolution of the $z(hb)$ ($z(hb) = X_{Na}, M4$), $y(hb) = Al^{VI}$ and $a(hb)$ ($a(hb) = X_{Na}, A$), in the P – T space.

the surface (the eclogites did not have enough time to re-equilibrate thermally). After the isothermal decompression, the geothermic gradients became normal so the decrease in pressure is accompanied with a decrease in temperature.

7. Conclusions

The eclogites of the Tighsi area represent a very good example to study the exhumation of the high-pressure basic rocks; however, the prograde path has been totally erased during eclogitization and it is only shown by some inclusions of epidote in garnet and omphacite. The conditions of 19.6 kbar–694 °C are the highest obtained in the LATEA metacraton so far.

At the peak metamorphic conditions the eclogites were H_2O under saturated; however, during exhumation (retrograde path),

the H_2O infiltrates and the shear zones that bring up eclogites to the surface are the main carrier of water toward eclogite lenses.

The use of the thermodynamic modeling has allowed the investigation of the P – T path and the different reactions that happens during the exhumation; furthermore, the isopleths track the evolution of each mineral composition in relation with the pressure/temperature modification.

The clockwise P – T path of eclogite from the Tighsi (Egere-Aleksod terrane) is characteristic of a major burying of the crust during subduction or continental collision followed by exhumation which goes from 19.6 kbar–694 °C (60 km of deep) to 9.3 kbar–695 °C revealed by a spectacular range of reaction textures, particularly amphibole, diopside, plagioclase and ilmenite symplectites that replace the peak metamorphic mineral assemblage (garnet, omphacite, quartz, rutile).

Acknowledgements

We thank anonymous reviewers for their help and constructive criticism of the manuscript. We are extremely grateful to OPNA, ORGM and COMENA for logistic support during fieldwork. This publication is a contribution to CNEPRU Project entitled “Modélisation thermodynamique et implication géodynamique des zones de suture de haute pression du Hoggar”.

References

- Adjerid, Z., Ouzegane, K., Godard, G., Derridj, A., Kienast, J.R., 2012. Le Sérouènout : un fragment de lithosphère océanique subducté à haute pression, exhumé puis granulitisé à haute température. *Bulletin du Service Géologique National* 23 (3), 199–217.
- Berger, J., 2008. Les associations de roches basiques – ultrabasiques néoprotérozoïques d'Amalaoulaou (Gourma, Mali), du Tassendjanet (Hoggar occidental, Algérie) et cénozoïques du Saghro (Anti-Atlas, Maroc): témoins de l'évolution géodynamique de la ceinture péri-cratonique Ouest-africaine. PhD thesis, Bruxelles, 431p.
- Bertrand, J.M., 1974. Evolution polycyclique des gneiss précambriens de l'Aleksod (Hoggar central, Sahara algérien). Aspects structuraux, pétrologiques, géochimiques et géochronologiques. Thèse Etat University de Montpellier, Ed. C.N.R.S. (C.R.Z.A.), sér. Geol. no. 19, 350p.
- Bertrand, J.M., Caby, R., 1978. Geodynamic evolution of the Pan- African orogenic belt: a new interpretation of the Hoggar shield (Algerian Sahara). *Geol. Rundschau* 67, 357–388.
- Bertrand, J.M., Lasserre, M., 1973. Pan-African and pre-Pan-African history of the Hoggar (Algerian Sahara) in the light of new geochronological data from the Aleksod area. – Precambrian. Research. 343–362.
- Black, R., Ba, A., Ball, E., Bertrand, J.-M., Boullier, A.M., Caby, R., 1979. Outline of the Pan-African Geology of Adrar des Iforas (Republic of Mali). *Geol. Rundschau* 68, 543–564.
- Black, R., Liégeois, J.P., Latouche, L., Caby, R., Bertrand, J.M., 1994. Pan-African displaced terranes in the Tuareg shield (Central Sahara). *J. Geol.* 22, 641–644.
- Bonhomme, M., 1962. Contribution à l'étude géochronologique de la plate-forme de l'Ouest Africain. Thèse Univ. Sci. Clermont-Ferrand, 62p.
- Briedj, M., 1993. Etude géologique de la région de Tahifet (Hoggar central, Algérie) implications géodynamiques. Thesis, University of Nancy 1, France, p. 201 (unpublished).
- Caby, R., Bertrand, J.M., Black, R., 1981. Pan-African ocean closures in the Hoggar-Iforas segment, Central Sahara. In: Kroner, A. (Ed.), *Precambrian Plate Tectonics*. Elsevier, Amsterdam, pp. 407–433.
- Chakraborty, S., Ganguly, G., 1991. Compositional zoning and cation diffusion in aluminosilicate garnets. In: Ganguly, J. (Ed.), *Diffusion, Ordering and Mass Transport in Physical Geochemistry*, Springer, vol. 8. Berlin, Heidelberg, New York, Tokyo, pp. 120–175.
- Coleman, R.G., Beatty, L.B., Brannock, W.W., 1965. Eclogites and eclogites: their differences and similarities. *Geol. Soc. Am. Bull.* 76, 483–508.
- Derridj, A., Ouzegane, K., Adjerid, Z., Godard, G., Kienast, J.R., 2010. Les éclogites granulitisées de ti-n-eggoleh (terrane du sérouènout, hoggar central): étude métamorphique et conséquence géodynamique. *Bulletin du Service Géologique National* 21 (2), 117–136.
- Diener, J.F.A., Powell, R., 2010. Influence of ferric iron on the stability of mineral assemblages. *J. Metamorph. Geol.* 28, 599–613.
- Diener, J.F.A., Powell, R., 2012. Revised activity–composition models for clinopyroxene and amphibole. *J. Metamorph. Geol.* 30, 131–142.
- Diener, J.F.A., Powell, R., White, R.W., Holland, T.J.B., 2007. A new thermodynamic model for clino- and orthoamphiboles in the system $\text{Na}_2\text{O}-\text{CaO}-\text{FeO}-\text{MgO}-\text{Al}_2\text{O}_3-\text{SiO}_2-\text{H}_2\text{O}-\text{O}$. *J. Metamorph. Geol.* 25, 631–656.
- Duplan, L., 1972. La chaîne de l'Egéré (Hoggar septentrional). *Bulletin du Service géologique de l'Algérie* 357p.
- Fettous, E., 2002. Les cisaillements lithosphériques en conditions anhydres et hydratées: exemples du Hoggar-Algerie. Magister USTHB, 209p.
- Green, E.C.R., Holland, T.J.B., Powell, R., 2007. An order–disorder model for omphacitic pyroxenes in the system jadeite–diopside–hedenbergite–acmite, with applications to eclogitic rocks. *Am. Mineral.* 92, 1181–1189.
- Holland, T.J.B., Powell, R., 1998. An internally consistent thermodynamic data set for phases of petrological interest. *J. Metamorph. Geol.* 16, 309–343.
- Holland, T.J.B., Powell, R., 2003. Activity–composition relations for phases in petrological calculations: an asymmetric multicomponent formulation. *Contrib. Miner. Petrol.* 145, 492–501.
- Latouche, L., 1978. Etude pétrographique et structurale du Précambrien de la région des Gour Oumelalen (Nord-Est de l'Ahaggar, Algérie). Thèse d'Etat, Paris 255p.
- Lelubre, M., 1952. Recherche sur la géologie de l'Ahaggar central et occidental (Sahara central). *Bulletin Service géologique Algérie* 22, tome 1, 354p, tome 2, 387p.
- Liégeois, J.-P., Bertrand, J.-M., Black, R., 1987. The subduction- and collision-related Panafrican composite batholith of the Adrar des Iforas (Mali). *Geol. J.* 22, 185–211.
- Liégeois, J.-P., Latouche, L., Boughrara, M., Navez, J., Guiraud, M., 2003. The LATEA metacraton (Central Hoggar, Tuareg Shield, Algeria): behaviour of an old passive margin during the Pan-African orogeny. *J. Afr. Earth Sci.* 37, 161–190.
- Morimoto, N., 1988. Nomenclature of pyroxenes. *Mineral. Mag.* 52, 535–550.
- Powell, R., Holland, T.J.B., 1988. An internally consistent thermodynamic dataset with uncertainties and correlations: 3. Applications to geobarometry, worked examples and a computer program. *J. Metamorph. Geol.* 6, 173–204.
- Sautter, V., 1985. An eclogite paragenesis from the Aleksod basement, Central Hoggar, South Algeria. *Chem. Geol.* 50, 331–347.
- White, R.W., Powell, R., Holland, T.J.B., Worley, B.A., 2000. The effect of TiO_2 and Fe_2O_3 on metapelitic assemblages at greenschist and amphibolite facies conditions: mineral equilibria calculations in the system $\text{K}_2\text{O}-\text{FeO}-\text{MgO}-\text{Al}_2\text{O}_3-\text{SiO}_2-\text{H}_2\text{O}-\text{TiO}_2-\text{Fe}_2\text{O}_3$. *J. Metamorph. Geol.* 18, 497–511.
- White, R.W., Powell, R., Holland, T.J.B., 2007. Progress relating to calculation of partial melting equilibria for metapelites. *J. Metamorph. Geol.* 25, 511–527.
- Zetoutou, S., Ouzegane, K., Boubazine, S., Kienast, J.R., 2004. Azrou N' Fad (central Hoggar, Algeria) one of the deepest terranes of LATEA: arguments based on $P-T$ evolution in eclogites. *J. Afr. Earth Sci.* 39, 193–220.